Design and performance of a Tuned Vibration Absorber for a full-scale lightweight FRP pedestrian structure

Christian Gallegos-Calderón[1]; Javier Naranjo-Pérez[2]; Jaime H. García-Palacios[3]; and Iván M. Díaz[4]

ABSTRACT

Fiber-reinforced polymers (FRPs) have enabled to build lightweight footbridges, whose structural design is often governed by Serviceability Limit State. A suitable approach to avoid over dimensioning an FRP footbridge may be to adopt a motion-based design strategy, where excessive human-induced vibrations are mitigated through the installation of Tuned Vibration Absorbers (TVAs). Also, Human-Structure Interaction (HSI) plays a key role and should be considered to estimate accurately the structural response of lightweight footbridges and avoid over dimensioning TVAs. Thus, this paper presents the design, installation, and performance assessment of a passive inertial controller for completing the construction of a full-scale FRP pedestrian structure. Firstly, a general frequency-domain procedure to design TVAs for structures susceptible to HSI is proposed. The methodology considers a multi-objective optimization problem that minimizes simultaneously the structural response and the controller inertial mass. Secondly, the HSI load model of a bouncing pedestrian is identified experimentally to be used within the proposal to design TVAs. Thirdly, a TVA of 25 kg is designed, assembled and installed in the lightweight FRP structure employing the proposed procedure. Then, the enhancement of the dynamic response due to the controller is assessed considering a person bouncing and two flows of walking pedestrians. For the

[1]Ph.D. Researcher, E.T.S.I. Caminos, Canales y Puertos, Universidad Politécnica de Madrid, Calle Profesor Aranguren 3, 28040, Madrid, Spain. E-mail: christian.gallegos@upm.es

[2]Ph.D. Researcher, E.T.S. Ingeniería, Universidad de Sevilla, Camino de los Descubrimientos s/n, 41092, Seville, Spain. E-mail: jnaranjo3@us.es

[3]Associate Professor, E.T.S.I. Caminos, Canales y Puertos, Universidad Politécnica de Madrid, Calle Profesor Aranguren 3, 28040, Madrid, Spain. E-mail: jaime.garcia.palacios@upm.es

[4]Full Professor, E.T.S.I. Caminos, Canales y Puertos, Universidad Politécnica de Madrid, Calle Profesor Aranguren 3, 28040, Madrid, Spain. E-mail: ivan.munoz@upm.es

different load scenarios, the TVA exhibits an adequate behavior to mitigate the vertical acceleration, demonstrating the feasibility to deliver an ultra-lightweight FRP footbridge with an inertial controller to meet requirements at different limit states.

Keywords: FRP footbridge, Lightweight structure, Human-Structure Interaction, Vibration control, Tuned Vibration Absorber.

INTRODUCTION

Since 1990s, fiber-reinforced polymers (FRPs) have been increasingly used in the construction industry, either to rehabilitate existing infrastructure or build new load bearing structures (Bakis et al. 2002; Hollaway 2010). Hence, several composite applications are part of hundreds, up to thousands, bridge projects nowadays (Manalo et al. 2017; Kim 2019; Wei et al. 2019). Regarding FRP footbridges, proposed guidelines (ACMA 2010; CEN 2021c) address the structural design from a static point of view, barely considering effects from pedestrian dynamic actions. These facts together with the limited information about the measured response of real composite structures, suggests that engineers should carefully pre-dict the dynamic behavior of new FRP footbridges to fully exploit the potential of composite materials.

Given the high strength-to-weight ratio and inherent lightweight nature of composites, the design of FRP structures is often driven by Serviceability Limit State (SLS), either deflections (Triandafilou and O'Connor 2009) or vibrations (Živanović et al. 2014). Therefore, stiff composite structures have been conceived since the design stage, such as the Toyohashi footbridge (Kumada et al. 2009), the Hakui and Tsukuba pedestrian bridges (Fukada et al. 2011), the St Austell footbridge (Shave et al. 2010), or the Dover pedestrian structure (Russell et al. 2020). In other FRP footbridges, strategies to limit the structural response have been implemented during the construction stage. For example, Firth (2002) placed lami-nated timber parapet panels and a surface layer of interlocking rubber blocks to provide extra damping to the Halgavor suspension bridge. Sobrino and Pulido (2002) incorporated longitudinal tied elements and diagonal members to join the arches of the Lleida footbridge.

In the Wilcott suspension footbridge, the central panels of the deck were ballasted using mortar blocks, intending to increase the mass of the deck and separate the frequency of the vertical and torsional vibration modes (Votsis et al. 2017). Another alternative to deliver an FRP pedestrian structure may be through the adoption of a motion-based design approach. This procedure may be divided in two parts, static and dynamic analyses. In the first one, checks at Deflection SLS (DSLS) and Ultimate Limit State (ULS) are complied. Whereas in the second part, vibration controllers are designed and installed in the structure to meet requirements at Vibration SLS (VSLS). In this sense, adding non-structural mass or including more structural elements due to serviceability issues are avoided to deliver a lightweight footbridge.

Well-established design guidelines (Boniface et al. 2006; ISO 2007; Butz et al. 2008) for conventional footbridges may be employed to evaluate the structural response of FRP structures subjected to pedestrian actions. Even the recommendations of the new proposals for Eurocodes (CEN 2021a; CEN 2021b) could be used to predict the dynamic behavior of composite footbridges at VSLS. Nevertheless, these documents may not be suitable to analyze a lightweight FRP footbridge as their load models are based on data (forces) measured on rigid surfaces, such as force plates or treadmills. In contrast to concrete or steel footbridges, higher and less energetic harmonics of pedestrian actions may affect the dynamic behav-ior of composite bridges due to their low generalized modal masses (Živanović et al. 2014). Hence, a natural frequency of 5 Hz is no longer a valid threshold to indicate a good dynamic performance of a pedestrian structure. For instance, Ahmadi et al. (2018) obtained peak accelerations up to 3.30 m/s^2 when a single person crossed a 8.7-m long laboratory Glass FRP (GFRP) structure. The pedestrian walked on the bridge at a gait frequency around 1.90 Hz, so the third harmonic of the action was synchronized with the vertical vibration mode, whose natural frequency was at 5.60 Hz.

Human-Structure Interaction (HSI) is another important aspect to consider within the design of FRP footbridges since unrealistic high vibration amplitudes may be predicted if

this phenomenon is omitted (Renedo et al. 2020). That is, load models from existing design guidelines, which do not consider HSI, over predict the response of FRP pedestrian structures (Ahmadi et al. 2019; Gallegos-Calderón et al. 2021a). To account for HSI, Single-Degree-of-Freedom (SDOF) systems, such as Mass-Spring-Damper (MSD) systems or Mass-Spring-Damper-Actuator (MSDA) systems, have been commonly employed to represent pedestrians performing different actions (Jones et al. 2011; Shahabpoor et al. 2016). Dynamic parameters of the human body, such as mass (m_h), natural frequency (f_h), and damping ratio (ζ_h), are considered to define these SDOF systems. For the cable-stayed GFRP Aberfeldy footbridge, whose main span is 63 m, Silva et al. (2020) demonstrated that a good agreement between experimental and numerical results can be obtained when a walker is represented through a MSD system, regardless of the parameters adopted to describe the human body.

To control significant structural responses due to pedestrian actions, passive strategies and particularly Tuned Vibration Absorbers (TVAs) are the most widespread solution. The main advantage of these systems is their purely mechanical functioning with no need of power supply. Butz et al. (2008), Casado et al. (2013) and Van Nimmen et al. (2016) have reported some successful applications of TVAs oriented to mitigate human-induced vibrations on footbridges. When dealing with lightweight FRP structures susceptible to HSI, classical approaches to design a TVA, such as the proposal of Den Hartog (1934), may not be applicable since a resonant structure with low damping cannot be longer idealized. Furthermore, multiple load scenarios should be also assessed before selecting the parameters of a TVA to obtain a more effective and less sensitive-to-uncertainties performance. According to Díaz et al. (2021), accounting for HSI on an FRP footbridge could be also beneficial in terms of reducing the size of vibration control devices. As this aspect contributes to reduce the use of material, further cost-effective FRP footbridge projects may be achieved.

This paper presents the design and performance of a TVA for a 10-m long FRP footbridge, whose linear mass is only 80 kg/m. A general frequency-domain procedure to design TVAs for pedestrian structures is proposed considering a coupled human-structure-controller

system. The proposal includes a multi-objective optimization problem that accounts for the H-infinity (H_∞) norm of the sum of Transfer Functions (TFs) and the inertial mass of the control devices. The TFs represent uncertainties in the human-structure systems, and the maximum amplitude or H_∞ norm of the sum is used as an indicator that guarantees the controller performance for the frequency band of interest. In contrast to classical deterministic approaches, the proposal allows designing robustly TVAs considering uncertainties in the parameters of the structure and the pedestrian. As a result, an accurate footbridge response and a proper controller sizing can be obtained while accounting for HSI.

The HSI load model of a bouncing person on a flexible surface is also presented in this paper. This model, based on a MSDA system, is identified from experimental results on the FRP structure and employed within the proposed methodology to design a TVA. Once the inertial controller is assembled and installed on the footbridge, the reduction of the structural response is assessed accounting for a person bouncing at midspan and two Traffic Classes (TCs) of pedestrian streams walking on the bridge. The remainder of this paper is organized as follows: (i) the frequency-domain procedure to design TVAs is briefly described, (ii) the HSI load model of a bouncing person is identified, (iii) the obtained load model is used to design a TVA for the FRP footbridge, (iv) the inertial controller is installed on the structure, and (v) the reduction of the structural response due to the TVA is assessed. In the end, conclusions are drafted, and an Appendix presents the properties of the FRP elements that form the pedestrian structure.

TVA DESIGN PROCEDURE

In this section, the procedure to design a passive inertial controller in the frequency domain is described. The proposal employs an MSD system to depict the structure, an MSDA system to describe the pedestrian, and an MSD system to represent the TVA. The model of a coupled human-structure-controller system is firstly explained. Then, a multi-objective optimization problem to design robustly a TVA is presented.

System modelling

If a person bouncing at midspan of the footbridge is adopted as the load case to design the TVA, a Linear Time-Invariant (LTI) system can be assumed, and a constant closed-loop TF can be obtained. This allows a fully frequency-domain analysis of the dynamic problem. Fig. 1a displays a representation of the human-structure-controller system, and Fig. 1b shows the corresponding block diagram. The LTI system is characterized by two feedback loops associated to the interaction phenomenon and the TVA, respectively.

The total closed-loop TF between the footbridge acceleration at midspan ($\ddot{x}_s$) and the human driving force (F_a), derived from Fig. 1b, in the Laplace domain may be expressed as follows

$$G_{CL}(s) = \frac{s^2 X_s(s)}{F_a(s)} = \frac{G_H(s) \cdot G_S(s)}{1 + G_S(s) \cdot \Big(G_{HSI}(s) + G_T(s)\Big)} \tag{1}$$

where $s = j\omega$ is the Laplace variable, ω (rad/s) is the angular frequency, $s^2 X_s(s)$ is the Laplace transform of the structural acceleration, $X_s(s)$ is the Laplace transform of the structural displacement, $G_S(s)$ is the TF related to the structural system, $G_H(s)$ is the TF between the human driving force and the contact force of the human with the structure, $G_{HSI}(s)$ is the TF related to HSI, and $G_T(s)$ is the TF associated to the inertial controller. Note that F_a is a pair of forces, and further explanation about obtaining these TFs can be found in Díaz et al. (2021).

For modeling the structure, the MSD system is defined considering the generalized modal mass, m_s (kg), the natural frequency, f_s (Hz), and the damping ratio, ζ_s, of a certain vibration mode. The TF of this system may be expressed as follows

$$G_S(s) = \frac{s^2 X_s(s)}{F_h(s)} = \frac{1/m_s\, s^2}{s^2 + 2\omega_s \zeta_s\, s + \omega_s^2} \tag{2}$$

where $\omega_s = 2\pi f_s$ (rad/s) is the angular natural frequency of the structure, and $F_h(s)$ is the Laplace transform of the resulting force acting on the structure.

For modeling the pedestrian, the MSDA system is defined by means of the mass, m_h (kg), natural frequency, f_h (Hz) and damping ratio, ζ_h, of the human body. When considering HSI, the human-structure system is described by two TFs. The first TF is associated to the force generated by the pedestrians without the structure movement (F_{ha}) and F_a, and it may be expressed as follows

$$G_H(s) = \frac{F_{ha}(s)}{F_a(s)} = \frac{-s^2}{s^2 + 2\omega_h\zeta_h\, s + \omega_h^2} \tag{3}$$

where $\omega_h = 2\pi f_h$ (rad/s) is the angular frequency of the human body. The second TF is related to the human interacting force (F_{hsi}) and the acceleration of the structure, and it is presented below

$$G_{HSI}(s) = \frac{F_{hsi}(s)}{s^2 X_s(s)} = \frac{m_h\,(2\omega_h\zeta_h\, s + \omega_h^2)}{s^2 + 2\omega_h\zeta_h\, s + \omega_h^2}. \tag{4}$$

For modeling the TVA, the MSD system is described through the inertial mass, m_t (kg), the natural frequency, f_t (Hz), and the damping ratio, ζ_t, of the device. The TF between the control force entering the structure (F_t) and the structural acceleration is as follows

$$G_T(s) = \frac{F_t(s)}{s^2 X_s(s)} = \frac{m_t\,(2\omega_t\zeta_t\, s + \omega_t^2)}{s^2 + 2\omega_t\zeta_t\, s + \omega_t^2} \tag{5}$$

where $\omega_t = 2\pi f_t$ (rad/s) is the angular frequency of the TVA.

Finally, the harmonic force (actuator force) generated by the pedestrian legs, disregarding the static load term, is expressed as follows

$$F_a = W_h \sum_{r=1}^{N_r} \mathrm{GLF}_r \sin(r \cdot 2\pi f_a) \tag{6}$$

with $r = 1,\ 2,\ \ldots\ N_r$, where N_r is the number of considered harmonics, W_h is the weight of the pedestrian, GLF_r is the Generated Load Factor associated to the rth harmonic, and f_a is the excitation frequency of the human action. Since the human driving force acts

simultaneously on the structure and the person, F_a employs GLFs (Dougill et al. 2006) instead of the Dynamic Load Factors typically used to define non-interacting load models in Boniface et al. (2006), ISO (2007), and Butz et al. (2008).

Control design methodology

The design of a TVA for a lively responsive footbridge is faced herein through a multi-objective optimization problem, which employs the total TF of the human-structure-controller system (Eq. 1). Two objectives are meant to be minimized, and the fulfillment of the VSLS is the adopted criterion to select the best solution among the set of optimum results.

Considering the fundamental vibration mode of the structure, one pedestrian acting on the bridge, and one TVA, this methodology uses the following vectors

$$\underline{z}_s = [m_s, f_s, \zeta_s] \tag{7}$$

where $\underline{z}_s$ is the vector containing the modal parameters of the structure,

$$\underline{z}_h = [m_h, f_h, \zeta_h] \tag{8}$$

where $\underline{z}_h$ is the vector containing the parameters of the human body, and

$$\underline{z}_t = [m_t, f_t, \zeta_t] \tag{9}$$

where $\underline{z}_t$ is the vector containing the parameters of the vibration controller.

Accounting for the aforementioned vectors, the multi-objective problem is formulated as follows

$$\min_{\underline{z}_t} \Big(J_1(\underline{z}_s, \underline{z}_h, \underline{z}_t),\ J_2(\underline{z}_t) \Big) \tag{10}$$

subjected to

$$\underline{z}_t \in [\underline{z}_{t,\min},\, \underline{z}_{t,\max}] \tag{11}$$

where J_1 and J_2 are the two objective functions to be minimized, and subscripts min and max indicate the minimum and maximum limits, respectively, for the search domain of $\underline{z}_t$. To consider uncertainties in the parameters of the structure and the interaction phenomenon, $\underline{z}_s$ and $\underline{z}_h$ may be described through statistical distributions. This leads to a robust design of TVAs and the fulfillment of the requirement at VSLS with a low probability of failure.

The objective function J_1 is

$$J_1(\underline{z}_s, \underline{z}_h, \underline{z}_t) = \max_{\omega} \sum_{p=1}^{P} \left| G_{CL}(\underline{z}_s, \underline{z}_h, \underline{z}_t, \omega) \right|_p \tag{12}$$

where $p = 1,\, 2,\, \ldots\, P$, P being the number of multivariate stochastic samples generated by varying the parameters of the coupled system. J_1 is the H_∞ norm of the sum of stochastically generated TFs, so it is computed by adding all the $|G_{CL}|_p$ obtained for each pth sample.

The objective function J_2 is the inertial mass of the controller, and it is expressed as follows

$$J_2(\underline{z}_t) = m_t. \tag{13}$$

Once the multi-objective optimization problem is solved, the optimal solutions are presented through the Pareto Front. From these results, the best solution is selected in order to meet a desired degree of comfort at VSLS for a particular confidence level (n). This criterion is expressed as follows

$$\mathrm{a}_{\mathrm{peak},n\mathrm{th}} \leq \mathrm{a}_{lim} \tag{14}$$

where $\mathrm{a}_{\mathrm{peak},n\mathrm{th}}$ is the peak acceleration of the nth percentile related to an optimum solution of the Pareto front. Each one of these results is related to P multivariate stochastic samples. To compute the peak acceleration of each $|G_{CL}|_p$, F_a (Eq. (6)) is swept in the frequency domain assuming that the first harmonic of bouncing action is between $f_{a,\min}$ and $f_{a,\max}$.

These limits may be between 1 and 3 Hz (Duarte and Ji 2009). From this sweeping, the maximum acceleration is obtained as follows

$$\mathrm{a}_{\mathrm{peak}} = \max_{f_a} \left(\sum_{r=1}^{N_r} \left| G_{CL}(\underline{z}_S, \underline{z}_h, \underline{z}_t, r \cdot 2\pi f_a) \right| \cdot W_h \, \mathrm{GLF}_r \right) \tag{15}$$

$$\forall f_a \in [f_{a,\min}, f_{a,\max}]$$

then, the Cumulative Distributive Function (CDF) for the P samples is computed and the nth percentile is derived, obtaining the $\mathrm{a}_{\mathrm{peak},n\mathrm{th}}$ to be applied in the selection criterion.

This general frequency-domain procedure can be straightforwardly extended to account for more vibration modes of the structure, more pedestrians acting on the footbridge and more inertial controllers.

BOUNCING ACTION IDENTIFICATION

This section describes the full-scale FRP footbridge and identifies the HSI load model of a person bouncing. For the second purpose, the coefficients corresponding to the second (GLF_2) and third (GLF_3) harmonic proposed by Dougill et al. (2006) are estimated based on the experimental results obtained from a pedestrian bouncing at midspan of the FRP footbridge.

Description of the structure

Pultruded GFRP profiles and Carbon FRP (CFRP) strips, manufactured by Fiberline Composites A/S (2018), form the 10-m long footbridge studied in this paper. The cross section of the structure is presented in Fig. 2a, where the three main GFRP stringers (one I 300×150×15 and two U 300×90×15) are shown. These stringers are laterally restrained by GFRP cross beams (I 160×80×8) each 1.20 m along the bridge length. Also, the bridge deck is assembled with Plank HD panels, and the handrails are comprised of stainless steel cables crossing square hollow GFRP profiles (SHS 60×60× 5). The connections among the different GFRP elements are achieved through M10 stainless steel bolts, whereas M8 clamps

are employed for the deck-to-stringer joints. In Fig. 2b, the CFRP strips (E 139/90/4.9 and E 139/150/4.9) employed in the bridge are displayed. These elements are bonded to the top and bottom flanges of the three stringers along their entire length by means of the Sikadur-330 adhesive (Sika Services AG 2017). To obtain a simply supported structure, pinned and roller supports at the ends of the bridge are installed (Fig. 2c). The geometry of the profiles and the properties of the materials associated to the different FRP elements are described in Appendix I. Additionally, the static verifications of the ultra-lightweight structure at DSLS and ULS can be found in Gallegos-Calderón et al. (2021b).

Prior to tests involving pedestrians, the modal parameters of the first vibration mode of the FRP footbridge were obtained through an Experimental Modal Analysis (EMA). A piezoelectric accelerometer attached at midspan of the central stringer (Fig. 3a) and an electrodynamic shaker (APS 2013) in a fixed body mode (Fig. 3b) were employed for this purpose. A chirp waveform was generated as the input signal of the shaker, and its instantaneous frequency increased slowly and linearly from 6 to 9 Hz during 5 minutes. The experimental Frequency Response Function (FRF), which corresponds to the TF of G_S shown in Eq.(2), was derived using the footbridge response and the shaker force. This force was obtained by monitoring the instantaneous current of the electrodynamic device during the test. As a result, $m_s = 405$ kg, $f_s = 7.47$ Hz, and $\zeta_s = 1.40\%$ were identified to define the bridge fundamental vibration mode as a MSD system. A comparison between the experimental FRF and the analytical TF of the SDOF system is shown in Fig. 3c.

Experiments with a pedestrian bouncing

Two test subjects, whose weights are presented in Table 1, were asked to bounce at midspan of the FRP bridge at a frequency (f_a) of 2.50 Hz, aiming to synchronize the third harmonic of the action to the fundamental frequency of the footbridge. Hence, the vertical bending vibration mode of the footbridge is excited. The sensor displayed in Fig. 3a was employed to collect the acceleration response at midspan. Each person performed three experiments for 20 s, controlling the frequency of the action with a metronome. Fig. 4

displays one of the trials of each test subject.

The recorded signals were processed using a low-pass filter with a cut-off frequency at 9 Hz to consider only the contribution from the first three harmonics of the human action. Fig. 5 shows the experimental results, in the time and frequency domains, from the first trial carried out by both test subjects. The maximum response obtained in each test is presented in Table 1. Also, the peak of the 1s-running Root-Mean-Square (RMS) acceleration response, known as Maximum Transient Vibration Value (MTVV), is stated in this table. As expected, significant structural responses were recorded in all the experiments since bouncing is a quite energetic action applied on the most responsive location of this ultra-lightweight structure.

Load model identification

As the proposed frequency-domain procedure employs a MSDA system to represent a pedestrian, the numerical response of the FRP footbridge was firstly assessed considering the MSDA system proposed by Dougill et al. (2006). Note that an MSDA system is the only HSI load model mentioned in a guideline to asses the dynamic performance of pedestrian structures subjected to bouncing action (ISE 2008). Hence, the following data were used: $m_h =$ 66 kg, $f_h = 2.30$ Hz, $\zeta_h = 25\%$, $\text{GLF}_1 = 0.286$, $\text{GLF}_2 = 0.095$, and $\text{GLF}_3 = 0.033$. For the analysis, the block diagram shown in Fig. 1b was implemented in SIMULINK (Math-works 2019b) accounting for the modal parameters of the structure presented in the previous subsection and without considering the contribution of the TVA. The fourth-order Runge-Kutta formula was adopted as the solver method with a time step of 0.001 s. The calculated peak response and MTVV were 1.23 m/s^2 and 0.73 m/s^2, respectively. As the numerical results of the uncontrolled structure were considerably underestimated in comparison with the experimental measurements (Table 1), GLF_2 and GLF_3 were calibrated as described hereafter.

Based on the experimental results from the trials of the Test Subject 1 (Fig. 4a), GLF_2 and GLF_3 were identified through a single-objective optimization problem, formulated as follows

$$\min_{\underline{z}_{fac}} \left(J_3(\underline{z}_{fac}) \right) \tag{16}$$

subjected to

$$\underline{z}_{fac} \in [\underline{z}_{fac,\min},\, \underline{z}_{fac,\max}] \tag{17}$$

where J_3 is the objective function, $\underline{z}_{fac}$ is the vector containing the GLF_2 and GLF_3 to be obtained, and subscripts min and max indicate the minimum and maximum limits, respectively, for the search domain of $\underline{z}_{fac}$. As a steady-state response of the structure is expected due to bouncing, leading to the same peak value and MTVV regardless of the time instant, J_3 is defined as follows

$$J_3(\underline{z}_{fac}) = \frac{1}{2}\left[\frac{\mathrm{a_{peak,exp}} - \mathrm{a_{peak,num}}(\underline{z}_{fac})}{\mathrm{a_{peak,exp}}}\right]^2 + \frac{1}{2}\left[\frac{\mathrm{MTVV_{exp}} - \mathrm{MTVV_{num}}(\underline{z}_{fac})}{\mathrm{MTVV_{exp}}}\right]^2 \tag{18}$$

where $\mathrm{a_{peak,exp}}$ is the mean measured peak acceleration equal to 4.08 $\mathrm{m/s^2}$, $\mathrm{a_{peak,num}}$ is the maximum numerical response, $\mathrm{MTVV_{exp}}$ is the mean experimental value equal to 2.54 $\mathrm{m/s^2}$, and $\mathrm{MTVV_{num}}$ is the numerical result. The search domains for the load factors are $GLF_2 \in [0.01, 0.20]$, and $GLF_3 \in [0.01, 0.15]$

The Genetic Algorithm (GA), implemented in MATLAB (Mathworks 2019a), was used to solve the optimization problem setting an initial population size of 20 individuals, a fitness limit of 10^{-6}, and a maximum number of generations of 100. The algorithm was run one hundred times (GA1-GA100) to obtain a meaningful solution. As all the results led to values of the objective function J_3 lower than 3%, a single solution was calculated by averaging the obtained $\underline{z}_{fac}$. Thus, $GLF_2 = 0.189$ and $GLF_3 = 0.120$ were computed. In comparison with the factors from Dougill et al. (2006), the identified GLFs are higher. This is expected since the coefficients of the aforementioned study were derived from experimental data obtained by Parkhouse and Ewins (2006) on a force plate (rigid surface). In contrast, it can be assumed that the estimated GLFs are associated to a flexible surface given the lively response of the

316 FRP footbridge.

317 To validate the identified HSI model, the results from the experiments of the Test Sub-
318 ject 2 (Fig. 4b) were compared with the numerical predictions. Considering that the pedes-
319 trian mass from Dougill et al. (2006) is 66 kg and the mass of the Test Subject 1 is 71.8 kg
320 (Table 1), m_h was set equal to 63.2 kg ($68.8 \cdot 66/71.8$) for the analysis involving the Test
321 Subject 2. The obtained peak response was 3.88 m/s^2, whilst the MTVV was 2.48 m/s^2.
322 Considering that these values are quite similar to the mean experimental measurements (Ta-
323 ble 1), the obtained HSI model of a person bouncing is accepted. In the next section, this
324 load model is used to design a TVA.

325 DESIGN OF THE CONTROLLER

326 The frequency-domain framework described in the second section is employed together
327 with the identified bouncing model to design a TVA for the FRP structure. The uncertainties
328 associated to the modal parameters of the structure and the interaction phenomenon are also
329 introduced, and the multi-objective optimization problem with the corresponding results are
330 presented.

331 The motion-based design requires to set a degree of comfort at VSLS under a certain
332 load scenario. Hence, one person bouncing at midspan is selected as the load case. This
333 activity allows to obtain a LTI system since the person remains always in the same location.
334 Moreover, bouncing is on the safety side with respect to walking action since the person is
335 always exciting the structure at its most responsive point (i.e. midspan).

336 As bouncing can be considered a vandal action given it does not occur on a daily basis,
337 a minimum degree of comfort (Butz et al. 2008) is chosen as the requirement to be met at
338 VSLS. Therefore, the following limit is assumed

$$\mathrm{a}_{lim} = 2.50\,\mathrm{m/s^2}. \tag{19}$$

339

340 Finally, to select the best solution from the Pareto front, a confidence level $n = 98$ is

adopted ($a_{peak,98th}$) for the criterion of Eq. (14).

Uncertainties

FRPs have shown an acceptable performance in terms of durability without compromising the structural safety and serviceability of an in-service footbridge (Keller et al. 2007). However, environmental and physical conditions may influence the long-term behavior of a composite bridge. For example, Stratford (2012) observed significant changes on the modal parameters of Aberfeldy GFRP footbridge after twenty years in service. To account for the variation in the stiffness of the structural elements, flexibility of bolted connections, addition or removal of physical mass (replacement of deck panels or retrofitting), the modal parameters of the FRP structure were defined through statistical distributions. A normal distribution ($\mathcal{N}$) was adopted for the generalized modal mass. Whilst similarly to the stiffness and strength properties of FRPs (Zureick et al. 2006), the fundamental frequency and damping ratio were assumed to follow a two-parameter Weibull distribution ($\mathcal{W}$). Considering a COV of 5%, the modal parameters of the first vibration mode of the FRP structure were as follows, m_s: $\mathcal{N}(405, 20.3)$ kg, f_s: $\mathcal{W}(7.47, 0.37)$ Hz, and ζ_s: $\mathcal{W}(1.40, 0.07)$ %.

The definition of uncertainties associated to the dynamic parameters of a person bouncing were also considered given the variability of values reported in literature, specially for the frequency and damping ratio of the human body. For this reason, a uniform distribution ($\mathcal{U}$) was adopted for both properties. Based on Jones et al. (2011), the parameters of the human body were described as follows, m_h: $\mathcal{N}(70, 5)$ kg, f_h: $\mathcal{U}(1.5, 6.0)$ Hz, and ζ_h: $\mathcal{U}(20, 50)$ %.

TVA design

For the design of the TVA, it was assumed that the third harmonic ($N_r = 3$) of the action is always synchronized with the bridge fundamental frequency, and the GLFs that define F_a were 0.286, 0.189, and 0.120 for the first three harmonics of the excitation, respectively. Assuming that the statistical distributions of the structure and the human body are mutually independent, 500 multivariate stochastic samples (P) were generated using the Latin Hypercube Method. For the sake of illustration, Fig. 6a displays the TFs corresponding to

the first 50 uncontrolled samples of the 500 coupled systems. Whereas Fig. 6b shows the objective function J_1 represented by the H_∞ norm of the sum of the 50 TFs.

The search domains for the mass, frequency and damping ratio of the TVA were: $m_t \in [4-40]$ kg, $f_t \in [6-9]$ Hz, and $\zeta_t \in [0.02-0.15]$. To solve the optimization problem, the multi-objective GA implemented in MATLAB (Mathworks 2019a) was used, and an initial population of 100 individuals together with a maximum number of generations of 100 were considered. Fig. 7a displays the Pareto Front obtained after carrying out the optimization. The TVA with an inertial mass of 25.46 kg (TVA-25) is the best solution (controller) since it allows the fulfillment of the selection criterion (Eq. (14)) with the lowest mass value. The number next to the controller indicates the inertial mass. The designed parameters of this device were: $m_t = 25.46$ kg, $f_t = 7.47$ Hz, and $\zeta_t = 14.80\%$. Fig. 7b shows the sum of the 500 TFs corresponding to the uncontrolled and controlled systems. J_1 was reduced from 11.73 to 5.53 m/s^2/N due the TVA-25, whereas the $a_{peak,98th}$ decreased from 4.34 to 2.49 m/s^2.

TUNED VIBRATION ABSORBER

In this section, the installation and tuning of the designed TVA-25 on the lightweight FRP footbridge are described.

Installation

Based on the solution from the previous section, the controller with an inertial mass of 25.46 kg was assembled and installed on the composite footbridge. Fig. 8a shows a scheme of the TVA-25, whose elements are: steel plates (17 kg), carcass (8 kg), springs (4 units), rod to guide (4 units), an adjustable fluid viscous damper, and a base.

To install the TVA on the pedestrian structure, two GFRP U $120 \times 50 \times 6$ profiles spanning crossbeams as close as possible to the bridge midspan, were connected to the secondary elements by means of stainless steel bolts class A2-50. The total mass of the controller, accounting for all the components, was approximately 35 kg. Fig. 8b presents the

TVA-25 installed on the pedestrian structure. In the picture, it can be seen the fluid viscous damper adapted from a universal adjustable steering stabilizer damper for motorcycles.

To finish the structural design, static checks were carried out again considering a concentrated dead load of 0.55 kN (1.5×weight of the device) at midspan of the structure. Design verifications of the U profiles and main girders at ULS considering the weight of the controller were performed, obtaining satisfactory results. Therefore, the motion-based design was completed since the FRP footbridge with the TVA-25 meet all the requirements at DSLS, ULS, and VSLS.

Tuning

To account for this robust design, the TVA was experimentally tuned considering just one human-structure system. The parameters of the first vibration mode of the FRP structure with the identified HSI model of a bouncing person were employed to obtain a numerical TF of the considered coupled system. After installing the TVA, a trial-and-error procedure was conducted aiming to obtain an experimental FRF similar to the analytical TF. For this process, the equipment shown in Fig. 3a-b was used to carry out the EMA, while the damping of the fluid viscous damper was being adjusted. Again, the generated signal as input of the shaker was a chirp waveform with a frequency range between 6 and 9 Hz during 5 minutes in the experiments to account for nonlinearities associated to the input amplitude.

In Fig. 9, it can be seen that the controller is not perfectly tuned to the first vibration mode of the bare structure since the amplitudes of the two peaks of the TF are not the same. In this graph, a good agreement between the analytical TF and the experimetnal FRF is noticed. This means that the TVA is slightly detuned to account for that variation on the properties of the human-structure system over time.

CONTROLLER PERFORMANCE

This section presents the dynamic response of the FRP footbridge with the TVA-25 considering a person bouncing and two flows of walking pedestrians. Comparisons between the results before and after the installation of the controller are drawn for each case.

Person bouncing

Prior to performing the experiments, a numerical prediction of the response of the FRP footbridge with the TVA-25 was carried out considering the identified HSI load model. For the analysis, the block diagram shown in Fig. 1b was implemented in SIMULINK (Mathworks 2019b), and the fourth-order Runge-Kutta formula was adopted as the solver method with a time step of 0.001 s. This led to a peak response of 1.20 m/s^2 and an MTVV of 0.66 m/s^2. Besides, Eq. (15) was used considering the nominal parameters of the FRP footbridge and the model of a bouncing person, resulting in a maximum acceleration equal to 1.22 m/s^2.

To assess experimentally the vibration serviceability of the structure with the TVA-25, three trials were carried out with the Test Subject 1 bouncing at 2.50 Hz (Fig. 4a). The duration of each test was 20 s, and the accelerometer shown in Fig. 3a was employed to collect the response at midspan. Again, the recorded signals were processed using the low-pass filter with a cut-off frequency at 9 Hz. The results of the experiments are presented in Table 2, where the mean peak response and mean MTVV among the three trials were 1.21 m/s^2 and 0.61 m/s^2, respectively. Hence, it is considered that the numerical predictions, obtained using SIMULINK or Eq. (15), are in agreement with the experimental results as the discrepancies are not significant. Note that the numerical and experimental results correspond just to one human-structure system, where the model of the pedestrian corresponds to the Test Subject 1 and the parameters of FRP structure present no deterioration.

Stream of pedestrians

Two set of tests were conducted to determine the vibration serviceability enhancement of the structure due to the TVA-25. Three and eight people walking in a closed circuit over the footbridge deck were considered to represent weak and dense TCs, respectively. Fig. 10 displays these load scenarios, and Table 3 presents the total mass of the people involved in each load case. The pedestrian density (d) and the pedestrian-to-structure mass ratio accounting for the mass of the FRP footbridge are also mentioned in the table.

First, the response of the bare FRP footbridge due to walking pedestrians was determined, and then, the vibration levels of the structure with the controller were obtained. The duration of all the tests was 5 minutes, and the accelerometer attached to the bottom of the central stringer (Fig. 3a) was used to measure the structural response at midspan. For all cases, a zero-phase 4th order Butterworth filter with upper and lower cut-off frequencies at 1 Hz and 20 Hz, respectively, was employed to process the signals collected at a sampling frequency of 1000 Hz during the tests.

For the weak TC (Fig. 10a), the footbridge response obtained before the installation of the TVA is presented in Fig. 11a. The peak acceleration was 2.14 m/s^2, and the MTVV was 1.22 m/s^2. The latter may be employed for the assessment of the dynamic behaviour of a pedestrian structure, as suggested in ISO (2007). For the dense TC (Fig. 10b), the acceleration response of the FRP footbridge is displayed in Fig. 12a. The peak acceleration was 2.42 m/s^2, and the MTVV was 1.20 m/s^2. Note that the response of the uncontrolled FRP structure is mainly associated to the fourth harmonic of the walking pedestrians, as shown in Figs 11a and 12a. Although the fundamental frequency of the bare structure (7.47 Hz) is above the threshold of 5 Hz that establishes an acceptable dynamic performance of a footbridge, a significant response was measured under the action of walking pedestrian. This is expected due to the low generalized mass (405 kg) associated to the first vibration mode.

The vibration levels of the footbridge with the TVA-25 subjected to the weak TC are shown in Fig. 11b. The peak response and the MTVV were reduced to 1.11 m/s^2 and 0.48 m/s^2, respectively. Whilst for the structure with the controller under the action of the dense TC, a peak acceleration of 1.56 m/s^2 and an MTVV of 0.59 m/s^2 were recorded (Fig. 12b). Table 4 presents the degrees of comfort achieved due to the TVA-25 for each TC. In both crowd scenarios, the comfort level was improved from CL3 (a_{lim} = 2.50 m/s^2) to CL2 (a_{lim} = 1.00 m/s^2), achieving a reduction of 61% for the weak TC and 51% for the dense TC. To define the degree of comfort, the MTVV$\cdot$ $\sqrt{2}$ was used for comparison with the

acceleration limits established in design guidelines (Živanović and Pavia 2009; Russell et al. 2020).

In addition to the MTVVs, the CDF curves are also compared to quantify the enhancement of structural dynamic response due to the installed controller for the whole test. In Fig. 13, the CDFs of the absolute acceleration response for the weak and dense TCs are displayed. The limit for the maximum degree of comfort (CL1) is also marked in the graphs to indicate the % of time where the acceleration response is below 0.50 m/s^2. For the weak TC, the maximum comfort was achieved 93% of the time due to the contribution of the controller. Whereas vibrations levels were below 0.50 m/s^2, 86% of the time for the case with a dense TC.

To estimate the reduction of the vibration levels due to the installed controller, the total area between the CDF curve and the y-axis is employed. Thus, a single value can be obtained as follows

$$\text{Reduction}_{\text{CDF}} = \frac{\text{Uncontrolled CDF}_{\text{area}} - \text{Controlled CDF}_{\text{area}}}{\text{Uncontrolled CDF}_{\text{area}}}. \tag{20}$$

Employing Eq. (20) for the weak TC (Fig. 13a), the obtained reduction was 53%. Whilst 46% was the calculated value for the dense TC using the aforementioned expression and Fig. 13b. From these results, it is appreciated that the fewer pedestrians involved in a test, the higher the reduction achieved with the controller.

CONCLUSIONS

In this paper, the feasibility of adopting a motion-based design approach to construct an FRP footbridge has been demonstrated. Instead of adding non-structural mass or including other composite structural elements, a TVA with an inertial mass of 25 kg is in charge of mitigating the structural response associated to higher harmonics of human actions (3rd harmonic of a bouncing person and 4th harmonic of a walking pedestrian). As a result, an ultra-lightweight FRP footbridge has been obtained. To the best of the authors' knowledge,

this is the first application of a TVA for an FRP pedestrian structure.

A frequency-domain framework has been proposed to design an inertial controller for a lightweight pedestrian structure susceptible to the interaction phenomenon. This proposal employs a multi-objective optimization, taking advantage of a coupled human-structure-controller system. The proposed approach allows to define uncertainties related to the structure and the human body, so a robust design of a vibration controller can be achieved since several analyses are carried out. Additionally, the HSI load model of a person bouncing on a flexible surface has been identified based on experimental measurements. Using this load model and the proposed frequency-domain procedure, a TVA has been designed, assembled and installed in the lightweight FRP footbridge. Then, the enhancement of the structural response due to the TVA-25 has been assessed. For the case of a pedestrian bouncing, a minimum degree of comfort (CL3) has been achieved. Whilst for the experiments with flows of walking pedestrians, an improvement of the degree of comfort, from a minimum level (CL3) to a medium level (CL2), has been achieved.

In the future, implementing more advanced vibration control strategies on the lightweight FRP footbridge will be explored using the proposed frequency-domain approach. Eddy-current TVAs, which do not have springs and provide damping from permanent magnets, and semi-active TVAs, which incorporate magneto-rheological dampers, will be investigated as feasible alternatives to control the structural response. Also, the identified HSI load model of a person bouncing will be used to predict the response of other lively responsive structures to further validate it.

DATA AVAILABILITY STATEMENT

All data, models, and codes generated or used during the study appear in the published article.

ACKNOWLEDGEMENTS

The authors acknowledge the grant RTI2018-099639-B-I00,'Structural efficiency enhancement for bridges subjected to dynamic loading: integrated smart damper', funded by MCIN/

AEI/10.13039/501100011033 and by 'ERDF A way of making Europe'. Christian Gallegos-Calderón expresses his gratitude to the Secretariat of Higher Education, Science, Technology and Innovation of Ecuador (SENESCYT) for the scholarship CZ02-000167-2018. Javier Naranjo-Pérez thanks the Ministry of Universities of Spain for the grant funded through the program 'European Union - NextGenerationEU'.

APPENDIX I. PROPERTIES OF THE FRP ELEMENTS

Information related to the GFRP profiles and CFRP strips employed to build the footbridge is provided herein according to Fiberline Composites A/S (2018). loads considered to design the composite pedestrian bridge are presented in the following subsections. The cross-section geometrical properties of the FRP elements are listed below:

- I 300×150×15: $h = 300$ mm, $b_f = 150$ mm, $t_w = 15$ mm, $t_f = 15$ mm, $A = 8740$ mm^2, $A_w = 4280$ mm^2, $I_y = 119.0 \times 10^6$ mm^4, and $I_z = 8.54 \times 10^6$ mm^4
- U 300×90×15: $h = 300$ mm, $b_f = 90$ mm, $t_w = 15$ mm, $t_f = 15$ mm, $A = 6850$ mm^2, $A_w = 4050$ mm^2, $I_y = 81.2 \times 10^6$ mm^4, and $I_z = 4.18 \times 10^6$ mm^4
- I 160×80×8: $h = 160$ mm, $b_f = 80$ mm, $t_w = 8$ mm, $t_f = 8$ mm, $A = 2490$ mm^2, $A_w = 1220$ mm^2, $I_y = 9.66 \times 10^6$ mm^4, and $I_z = 0.69 \times 10^6$ mm^4
- SHS 60×60×5: $b = 60$ mm, $t = 5$ mm, $A = 1110$ mm^2, and $I_y = 0.57 \times 10^6$ mm^4
- Plank HD: $h = 40$ mm, and $w = 17.06$ kg/m^2
- CFRP strips: $b_C = 150$ mm or $b_C = 90$ mm depending on the width of the flanges of the stringers, and $t_C = 4.9$ mm

where h is the depth of the profile, b_f is the flange width, t_w is the web thickness, t_f is the flange thickness, A is the area of the cross-section, A_w is the cross-section area for shear, I_y and I_z are the moments of inertia with respect to the major and minor axis, respectively, w is the weight of a panel per square meter, b_C is the width of the strip, and t_C is the thickness of the strip. Additionally, the density values for the GFRP and CFRP are 1800 kg/m^3 and 1550 kg/m^3, respectively.

In Tables 5 and 6, relevant characteristic stiffness values and strength properties of the considered FRP elements are presented, respectively. In these tables, 'dir. 1' refers to the orientation of the material in the pultrusion direction, and 'dir. 2' is related to an orientation perpendicular to the pultrusion direction.

REFERENCES

ACMA (2010). *Pre Standard for Load and Resistance Factor Design (LRFD) of Pultruded Fiber Reinforced Polymer (FRP) Structures*. American Society of Civil Engineers ASCE (nov).

Ahmadi, E., Caprani, C., Živanović, S., and Heidarpour, A. (2018). "Vertical ground reaction forces on rigid and vibrating surfaces for vibration serviceability assessment of structures." *Engineering Structures*, 172, 723–738.

Ahmadi, E., Caprani, C., Živanović, S., and Heidarpour, A. (2019). "Assessment of human-structure interaction on a lively lightweight GFRP footbridge." *Engineering Structures*, 199, 109687.

APS (2013). *APS 400 ELECTRO-SEIS® - Long Stroke Shaker with Linear Ball Bearings*. APS Dynamics Inc.

Bakis, C. E., Bank, L. C., Brown, V. L., Cosenza, E., Davalos, J. F., Lesko, J. J., Machida, A., Rizkalla, S. H., and Triantafillou, T. C. (2002). "Fiber-Reinforced Polymer Composites for Construction—State-of-the-Art Review." *Composites for Construction*, 6(2), 73–87.

Boniface, V., Bui, V., Bressolette, P., Charles, P., and Cespedes, X. (2006). *Footbridges: Assessment of vibrational behaviour of footbridges under pedestrian loading*. Service d'Études Techniques des Routes et Autoroutes, Paris (oct).

Butz, C., Heinemeyer, C., Keil, A., Schlaich, M., Goldack, A., Trometer, S., Lukić, M., Chabrolin, B., Lemaire, A., Martin, P.-O., Cunha, Á., and Caetano, E. (2008). *HIVOSS: Design of footbridges guideline*. Research Fund for Coal and Steel.

Casado, C. M., Díaz, I. M., de Sebastián, J., Poncela, A. V., and Lorenzana, A. (2013). "Implementation of passive and active vibration control on an in-service footbridge." *Structural Control and Health Monitoring*, 20(1), 70–87.

CEN (2021a). *Draft prEN 1990:2021 Basis of Structural and Geotechnical Design, Annex A.2. Applications for Bridges*. European Committee for Standardisation (sep).

CEN (2021b). *Draft prEN 1991-2:2021: Actions on structures — Part 2: Traffic Loads on*

584 *Bridges and Other Civil Engineering Works*. European Committee for Standardization
585 (sep).
586 CEN (2021c). *Draft prTS 19101:2021 Design of fibre-polymer composite structures*. European
587 Committee for Standardization (oct).
588 Den Hartog, J. P. (1934). *Mechanical vibrations*. McGraw-Hill Book Company, New York.
589 Díaz, I. M., Gallegos-Calderón, C. A., Ramírez Senent, J., and Renedo, C. M. C. (2021).
590 "Interaction Phenomena to Be Accounted for Human-Induced Vibration Control of
591 Lightweight Structures." *Frontiers in Built Environment*, 7, 49.
592 Dougill, J. W., Wright, J. R., Parkhouse, J. G., and Harrison, R. E. (2006). "Human structure
593 interaction during rhythmic bobbing." *The Structural Engineer*, 32–39.
594 Duarte, E. and Ji, T. (2009). "Action of Individual Bouncing on Structures." *Journal of*
595 *Structural Engineering*, 135(7), 818–827.
596 Fiberline Composites A/S (2018). *General Design Certification*. Fiberline Composites A/S,
597 Middelfart, Denmark (may).
598 Firth, I. (2002). "A Tale of Two Bridges: The Lockmeadow and Halgavor bridges." *The*
599 *Institution of Structural Engineers*, (5), 26–332.
600 Fukada, S., Kajikawa, Y., Nishizaki, I., Kishima, T., and Hosonuma, H. (2011). "Vibration
601 characteristics and serviceability of the FRP girder bridge." *2nd International MultiCon-*
602 *ference on Complexity, Informatics and Cybernetics*, Orlando, FL.
603 Gallegos-Calderón, C., Naranjo-Pérez, J., Díaz, I. M., and Goicolea, J. M. (2021a). "Identi-
604 fication of a human-structure interaction model on an ultra-lightweight FRP footbridge."
605 *Applied Sciences*, 11(14), 6654.
606 Gallegos-Calderón, C., Naranjo-Pérez, J., Pulido, M. D. G., and Díaz, I. M. (2021b). "Design,
607 construction and structural response of a lightweight FRP footbridge." *IABSE Congress:*
608 *Structural Engineering for Future Societal Needs*, Ghent, 2053–2061 (sep).
609 Hollaway, L. C. (2010). "A review of the present and future utilisation of FRP compos-
610 ites in the civil infrastructure with reference to their important in-service properties."

Construction and Building Materials, 24(12), 2419–2445.

ISE (2008). *Dynamic performance requirements for permanent grandstands subject to crowd action: Recommendations for management, design and assessment*. Institution of Structural Engineers, London, UK (dec).

ISO (2007). *ISO 10137 - Bases for design of structures - Serviceability of buildings and walkways against vibrations*, Vol. 10137. International Organization for Standardization.

Jones, C. A., Reynolds, P., and Pavic, A. (2011). "Vibration serviceability of stadia structures subjected to dynamic crowd loads: A literature review." *Journal of Sound and Vibration*, 330(8), 1531–1566.

Keller, T., Bai, Y., and Vallée, T. (2007). "Long-Term Performance of a Glass Fiber-Reinforced Polymer Truss Bridge." *Journal of Composites for Construction*, 11(1), 99–108.

Kim, Y. J. (2019). "State of the practice of FRP composites in highway bridges." *Engineering Structures*, 179, 1–8.

Kumada, T., Yamada, S., Johansen, E., and Wilson, R. (2009). " Static and dynamic behavior of a pultruded FRP truss footbridge." *2nd Official International Conference of International Institute for FRP in Construction for Asia-Pacific Region*, Seoul, South Korea, 355–361 (dec).

Manalo, A., Aravinthan, T., Fam, A., and Benmokrane, B. (2017). "State-of-the-Art Review on FRP Sandwich Systems for Lightweight Civil Infrastructure." *Journal of Composites for Construction*, 21(1), 16.

Mathworks (2019a). *MATLAB - Getting Started Guide*. Matick.

Mathworks (2019b). *Simulation and Model-Based Design - Documentation*. Matick.

Parkhouse, J. G. and Ewins, D. J. (2006). "Crowd-induced rhythmic loading." *Proceedings of the Institution of Civil Engineers - Structures and Buildings*, 159(5), 247–259.

Renedo, C. M., Díaz, I. M., Russell, J. M., and Živanovic, S. (2020). "Performance of inertial mass controllers for ultra-lightweight footbridges: A case study." *xi International*

Conference on Structural Dynamics EURODYN, Vol. 1, Athens, Greece, 1741–1746 (nov).

Russell, J., Wei, X., Živanović, S., and Kruger, C. (2020). "Vibration serviceability of a GFRP railway crossing due to pedestrians and train excitation." *Engineering Structures*, 219, 110756.

Shahabpoor, E., Pavic, A., and Racic, V. (2016). "Interaction between Walking Humans and Structures in Vertical Direction: A Literature Review." *Shock and Vibration*, 2016, 1–22.

Shave, J., Denton, S., and Frostick, I. (2010). "Design of the St Austell fibre-reinforced polymer Footbridge, UK." *Structural Engineering International*, 20(4), 427–429.

Sika Services AG (2017). *Sikadur-330 Data Sheet*. Zürich, Switzerland (aug).

Silva, R., Pimentel, R. L., and Pavic, A. (2020). "Performance of biodynamic models to represent the action of a pedestrian in the vertical direction." *XI International Conference on Structural Dynamic , EURODYN*, Vol. 40, Athens, Greece, 1824–1834 (nov).

Sobrino, J. A. and Pulido, M. D. G. (2002). "Towards Advanced Composite Material Footbridges." *Structural Engineering International*, 12(2), 84–86.

Stratford, T. (2012). "The condition of the Aberfeldy Footbridge after 20 years in service." *Structural Faults and Repair*, Edinburgh, UK (jul).

Triandafilou, L. N. and O'Connor, J. S. (2009). "FRP Composites for Bridge Decks and Superstructures: State of the Practice in the U.S.." *International Conference on Fiber Reinforced Polymer (FRP) Composites for Infrastructure Applications*, Stockton.

Van Nimmen, K., Verbeke, P., Lombaert, G., De Roeck, G., and Van den Broeck, P. (2016). "Numerical and Experimental Evaluation of the Dynamic Performance of a Footbridge with Tuned Mass Dampers." *Journal of Bridge Engineering*, 21(8), C4016001.

Votsis, R. A., Stratford, T. J., Chryssanthopoulos, M. K., and Tantele, E. A. (2017). "Dynamic assessment of a FRP suspension footbridge through field testing and finite element modelling." *Steel and Composite Structures*, 23(2), 205–215.

Wei, X., Russell, J., Živanović, S., and Toby Mottram, J. (2019). "Measured dynamic properties for FRP footbridges and their critical comparison against structures made of con-

665 ventional construction materials." *Composite Structures*, 223, 110956.
666 Živanović, S., Feltrin, G., Mottram, J. T., and Brownjohn, J. M. (2014). "Vibration perfor-
667 mance of bridges made of fibre reinforced polymer." *Conference Proceedings of the Society*
668 *for Experimental Mechanics Series*, Vol. 4, Orlando, FL, 155–162.
669 Živanović, S. and Pavia, A. (2009). "Probabilistic Assessment of Human Response to Foot-
670 bridge Vibration." *Low Frequency Noise, Vibration and Active Control*, 28(4), 255–268.
671 Zureick, A. H., Bennett, R. M., and Ellingwood, B. R. (2006). "Statistical characterization
672 of fiber-reinforced polymer composite material properties for structural design." *Journal*
673 *of Structural Engineering*, 132(8), 1320–1327.

NOTATION

The following symbols are used in this paper:

A = cross-section area (mm^2);

A_w = cross-section area for shear (mm^2);

a_{lim} = acceleration limit (m/s^2);

a_{peak} = maximum acceleration (m/s^2);

$a_{peak,nth}$ = peak acceleration of the nth percentile (m/s^2);

b_C = strip width (mm);

b_f = flange width (mm);

d = density of pedestrians (pedestrians/m^2);

E_{c1} = compressive modulus of GFRP in direction 1 (GPa);

E_{c2} = compressive modulus of GFRP in direction 2 (GPa);

E_{t1} = tensile modulus of GFRP in direction 1 (GPa);

E_{t1C} = tensile modulus of CFRP in direction 1 (GPa);

E_{t2} = tensile modulus of GFRP in direction 2 (GPa);

F_{c1} = compressive strength of GFRP in direction 1 (MPa);

F_{c1C} = compressive strength of CFRP in direction 1 (MPa);

F_{c2} = compressive strength of GFRP in direction 2 (MPa);

F_{f1} = flexural strength of GFRP in direction 1 (MPa);

F_{f2} = flexural strength of GFRP in direction 2 (MPa);

F_h = resulting force acting on the structure (N);

F_{ha} = human force without considering the structure movement (N);

F_{hsi} = human interacting force (N);

F_{p1} = pin bearing strength of GFRP in direction 1 (MPa);

F_{p2} = pin bearing strength of GFRP in direction 2 (MPa);

F_{T12} = shear strength perpendicular to the plane 12 (MPa);

F_t = force transmitted from the TVA to the structure (N);

F_{t1} = tensile strength of GFRP in direction 1 (MPa);

F_{t1C} = tensile strength of CFRP in direction 1 (MPa);

F_{t2} = tensile strength of GFRP in direction 2 (MPa);

F_{12} = in-plane shear strength (MPa);

F_6 = interlaminar shear strength (MPa);

f_a = frequency of the human action (Hz);

f_h = natural frequency of the person (Hz);

f_s = natural frequency of the structure (Hz);

f_t = natural frequency of the TVA (Hz);

GLF = Generated load factor;

G_{CL} = TF of the human-structure-controller system ($m/s^2/N$);

G_S = TF of the structural system ($m/s^2/N$);

G_H = TF between the human driving force and F_{ha} (N/N);

G_{HSI} = TF related to the interaction phenomenon ($N/m/s^2$);

G_T = TF of the inertial controller ($N/m/s^2$);

G_{12} = in-plane shear modulus (GPa);

H_∞ = maximum value of a TF ($N/m/s^2$);

h = depth of a profile (mm);

I_y = moment of inertia of with respect to the major axis (mm^4);

I_z = moment of inertia with respect to the minor axis (mm^4);

J = objective function;

j = imaginary unit;

MTVV = Maximum transient vibration value (m/s^2);

m_h = mass of the pedestrian (kg);

m_s = modal mass of the structure (kg);

m_t = inertial mass of the TVA (kg);

$\mathcal{N}$ = Normal distribution;

N_r = number of considered harmonics;

P = number of multivariate stochastic samples;

p = multivariate stochastic sample;

s = Laplace variable;

t_C = thickness of a strip (mm);

t_f = thickness of a flange (mm);

t_w = thickness a web, (mm);

$\mathcal{W}$ = Weibull distribution ;

W_h = weight of the pedestrian (N);

w = weight of a panel per unit of area (kg/m^2);

X_s = Laplace transform of the structural displacement;

$\ddot{x}_s$ = acceleration of the structure (m/s^2);

678 $\underline{z}_{fac}$ = vector containing GLF_2 and GLF_3;

$\underline{z}_h$ = vector containing the parameters of the human body;

$\underline{z}_s$ = vector containing the modal parameters of the structure;

$\underline{z}_t$ = vector containing the parameters of the TVA;

ω = angular frequency (rad/s);

ω_s = angular frequency of the structure (rad/s);

ω_h = angular frequency of the human body (rad/s);

ω_t = angular frequency of the TVA (rad/s);

ν_{12} = in-plane Poisson's ratio 12;

ν_{21} = in-plane Poisson's ratio 21;

ζ_h = damping ratio of the human body (%);

ζ_s = damping ratio of the structure (%); and

ζ_t = damping ratio of the TVA (%).

List of Tables

TABLE 1. Response of the FRP footbridge due to a pedestrian bouncing at 2.50 Hz

Test subject	Mass (kg)	Trial	a_{peak} (m/s^2)	MTVV (m/s^2)
1	71.8	1	3.84	2.39
		2	4.38	2.69
		3	4.02	2.53
		Mean	4.08	2.54
2	68.8	1	4.27	2.70
		2	3.38	2.16
		3	4.21	2.57
		Mean	3.95	2.48

TABLE 2. Response of the FRP footbridge with the TVA-25 due to the Test Subject 1 bouncing at 2.50 Hz

Test subject	Mass (kg)	Trial	a_{peak} (m/s^2)	MTVV (m/s^2)
1	71.8	1	1.14	0.52
		2	1.45	0.69
		3	1.03	0.62
		Mean	1.21	0.61

TABLE 3. Mass of walking pedestrians involved in the tests.

Traffic class	Number of pedestrians	d (pedestrians/m^2)	Total mass of pedestrians (kg)	Mass ratio
Weak	3	0.20	218.8	0.27
Dense	8	0.53	585.7	0.73

TABLE 4. Degree of comfort and reduction of vertical vibrations for both TCs

Traffic class	Uncontrolled		Controlled		Reduction (%)
	MTVV·$\sqrt{2}$ (m/s^2)	Comfort level	MTVV·$\sqrt{2}$ (m/s^2)	Comfort level	
Weak	1.73	CL3	0.68	CL2	61
Dense	1.70	CL3	0.83	CL2	51

TABLE 5. Characteristic stiffness values of the FRP elements

Material	Parameter	Symbol	Units	Value
GFRP	Tensile modulus, dir. 1	E_{t1}	GPa	24.0
	Tensile modulus, dir. 2	E_{t2}	GPa	7.0
	Compressive modulus, dir. 1	E_{c1}	GPa	24.0
	Compressive modulus, dir. 2	E_{c2}	GPa	10.0
	In-plane Poisson's ratio, 12	ν_{12}	-	0.23
	In-plane Poisson's ratio, 21	ν_{21}	-	0.07
	In-plane shear modulus	G_{12}	GPa	3.0
CFRP	Tensile modulus, dir. 1	E_{t1C}	GPa	139.0

TABLE 6. Characteristic strength values of the FRP elements

Material	Parameter	Symbol	Units	Value
GFRP	Tensile strength, direction 1	F_{t1}	MPa	240
	Tensile strength, direction 2	F_{t2}	MPa	35
	Compressive strength, direction 1	F_{c1}	MPa	240
	Compressive strength, dir. 2	F_{c2}	MPa	90
	Pin bearing strength, dir. 1	F_{p1}	MPa	200
	Pin bearing strength, dir. 2	F_{p2}	MPa	120
	Flexural strength, dir. 1	F_{f1}	MPa	240
	Flexural strength, dir. 2	F_{f2}	MPa	60
	Interlaminar shear strength	F_6	MPa	20
	Shear strength perpendicular to plane 12	F_{T12}	MPa	50
	In-plane shear strength	F_{12}	MPa	40
CFRP	Tensile strength, dir. 1	F_{t1C}	MPa	1640
	Compressive strength, dir. 1	F_{c1C}	MPa	890

List of Figures

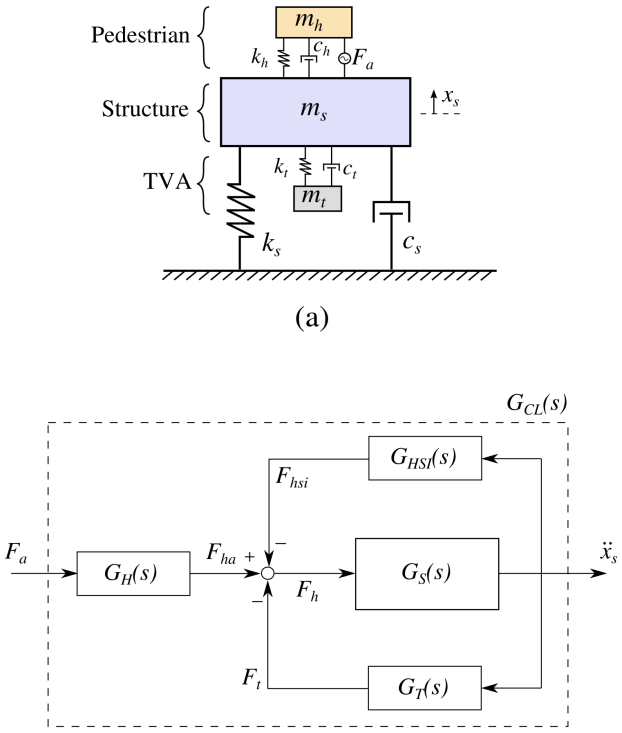

FIG. 1. Modeling: (a) Human-structure-controller system, and (b) Block diagram.

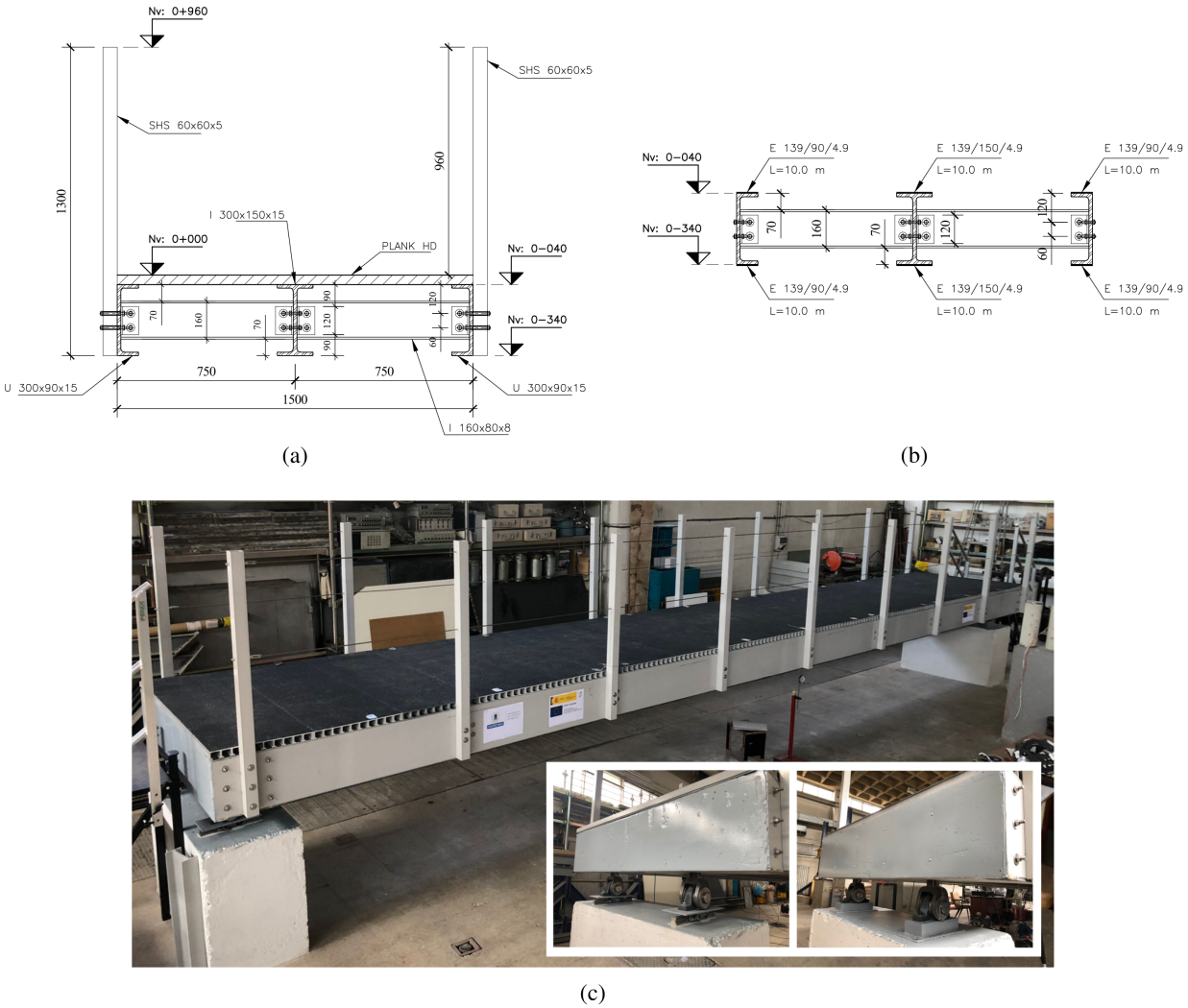

FIG. 2. Lightweight FRP footbridge: (a) Cross section, (b) Position of the CFRP strips, and (c) Built structure. All dimensions in mm.

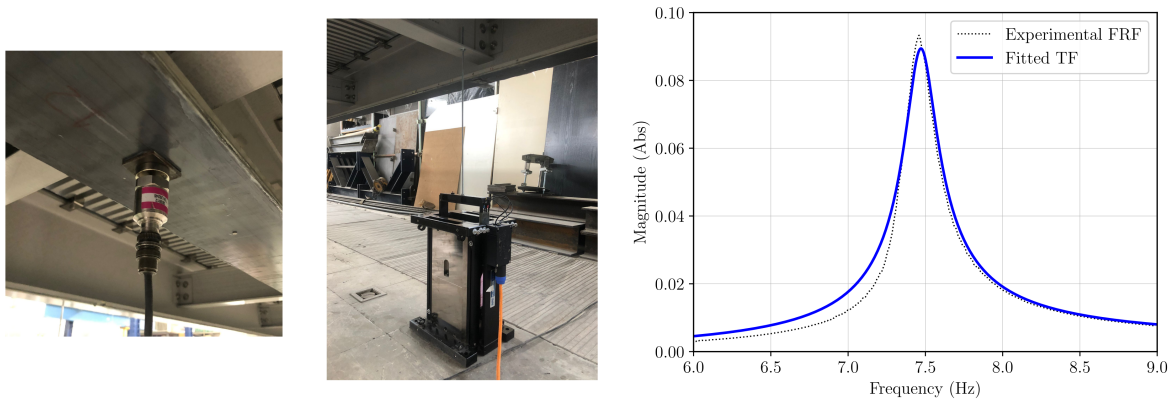

(a) (b) (c)

FIG. 3. Bare structure: (a) Accelerometer underneath the central stringer, (b) Electrodynamic shaker in a fixed body mode, and (c) Comparison of the experimental FRF and the analytical TF.

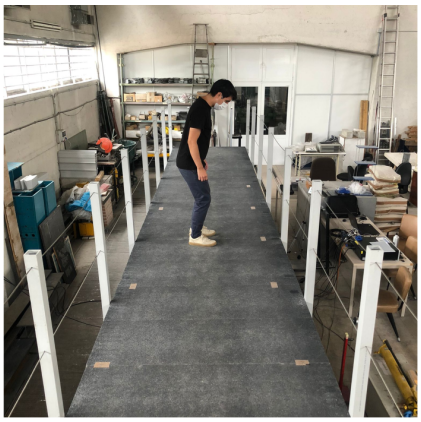

(a)

(b)

FIG. 4. Pedestrian bouncing at 2.50 Hz: (a) Test subject 1, and (b) Test subject 2.

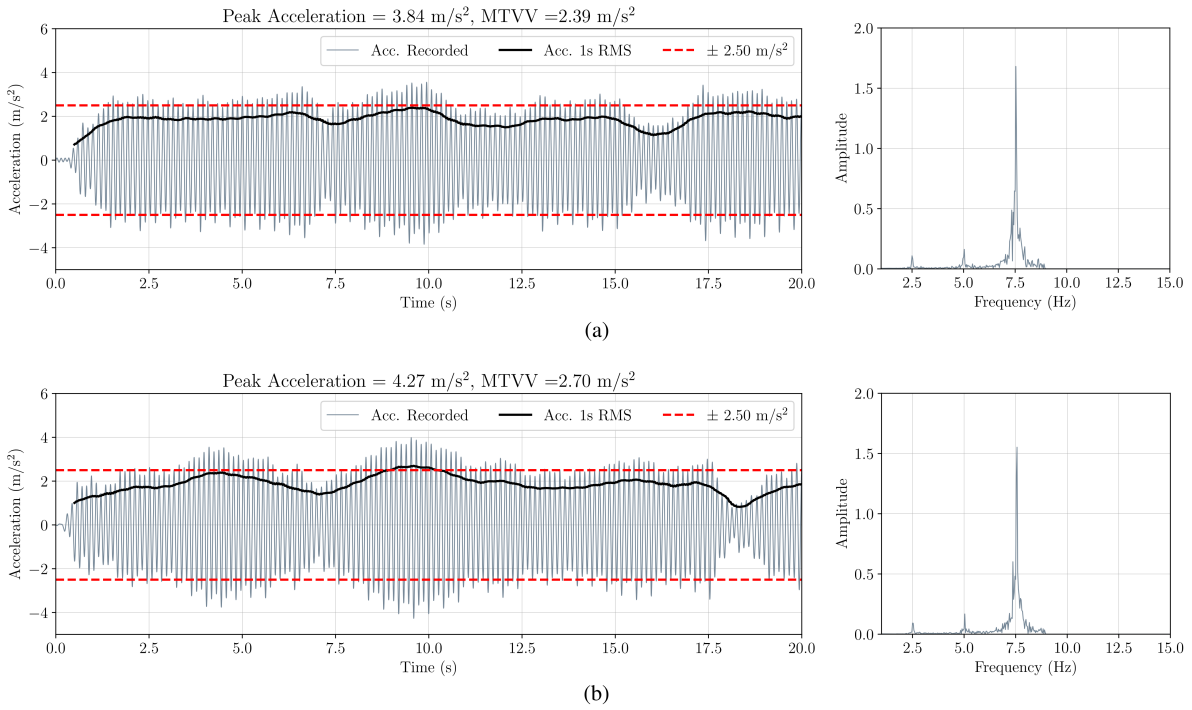

FIG. 5. Response at midspan due to a pedestrian bouncing at 2.50 Hz: (a) Test subject 1, and (b) Test subject 2.

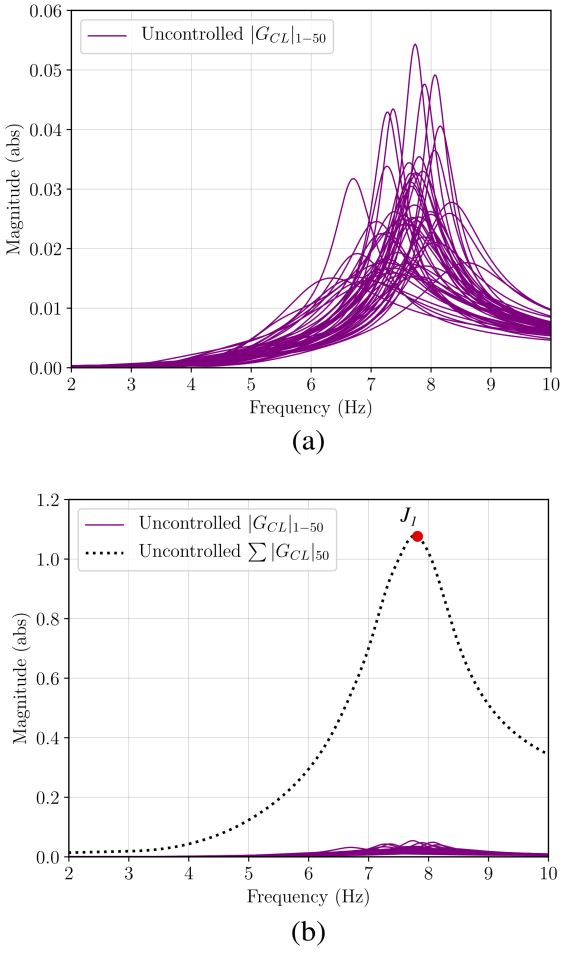

FIG. 6. Multivariate stochastic systems: (a) Uncontrolled 50 coupled systems, and (b) Representation of J_1.

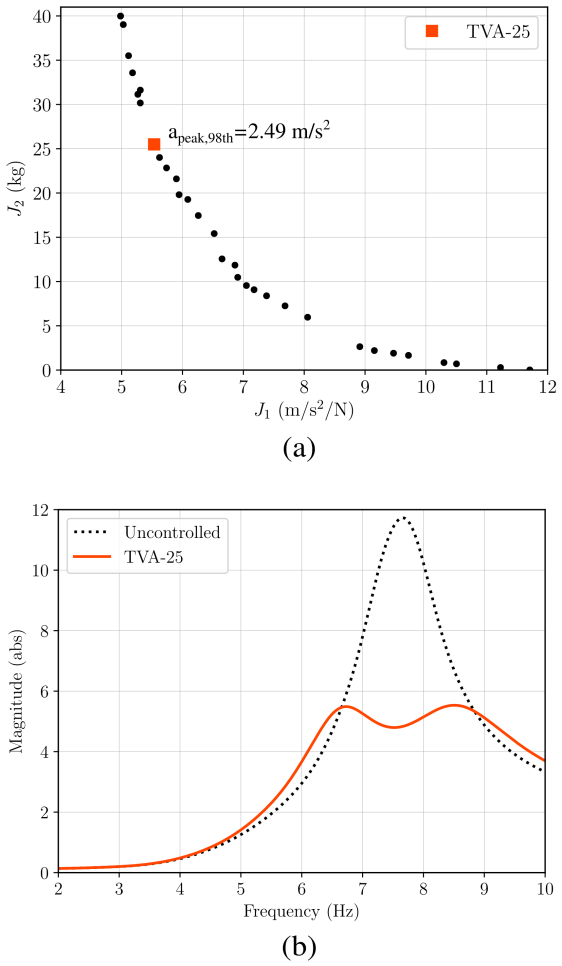

FIG. 7. Design results: (a) Pareto front, and (b) Comparison of cumulative functions.

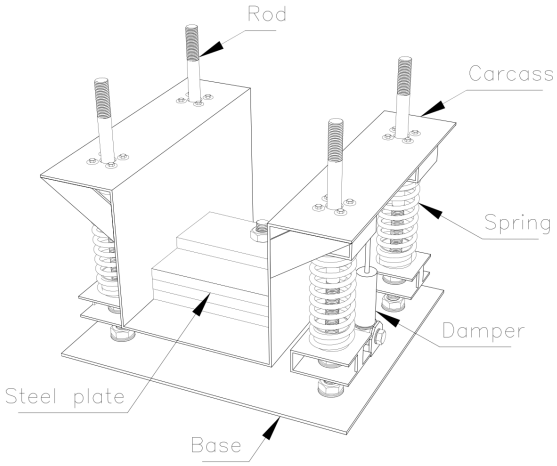

(a)

(b)

FIG. 8. TVA-25: (a) Mechanical design, and (b) Controller installed underneath the structure.

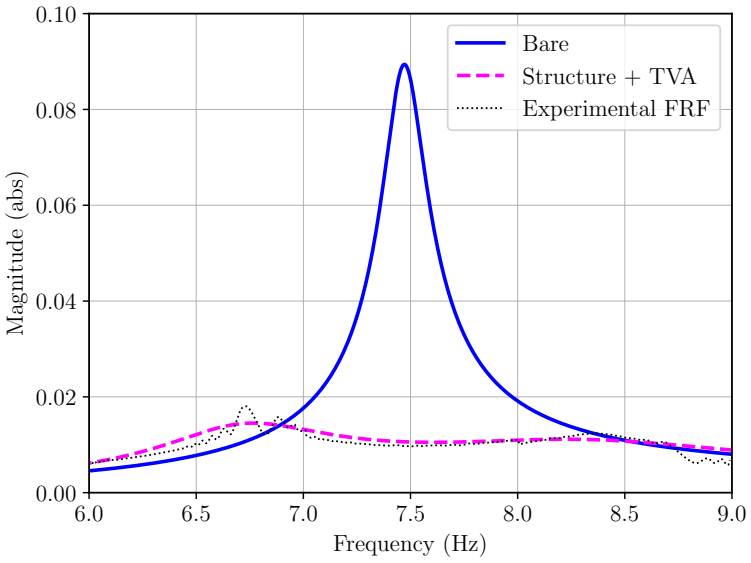

FIG. 9. Tunning of the TVA-25 to the fundamental vibration mode of the FRP structure.

(a)

(b)

FIG. 10. Tests with walking pedestrians: (a) Weak TC, and (b) Dense TC.

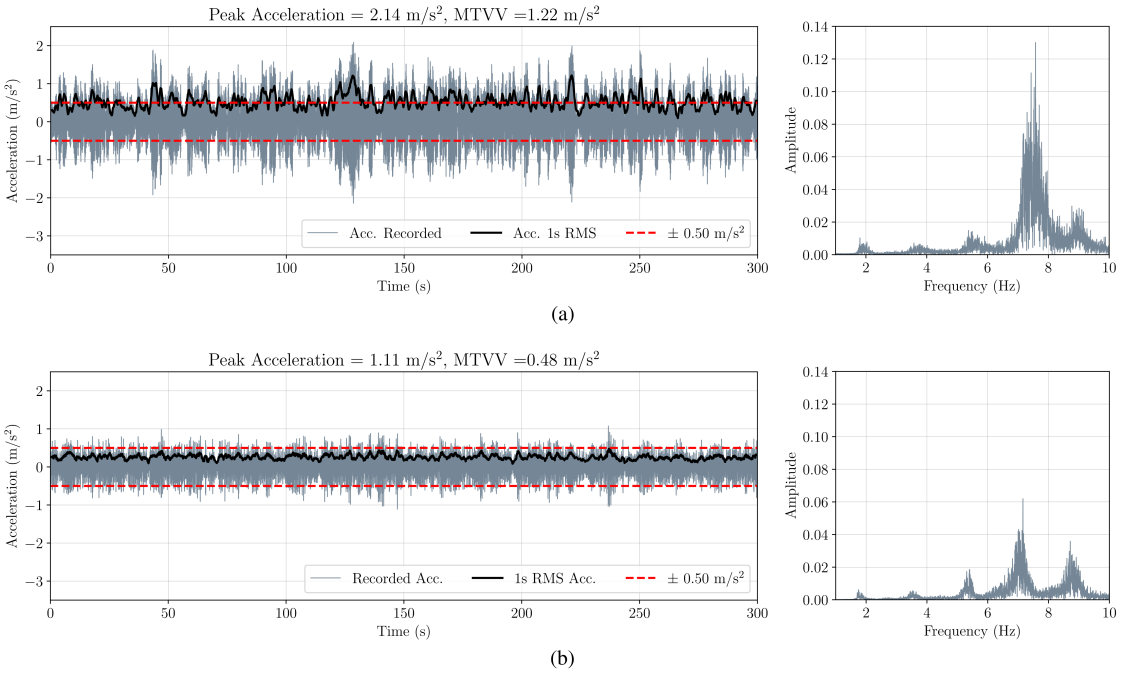

FIG. 11. Acceleration response of the FRP footbridge at midspan due to a weak TC: (a) Structure without control, and (b) Controlled structure with the TVA-25.

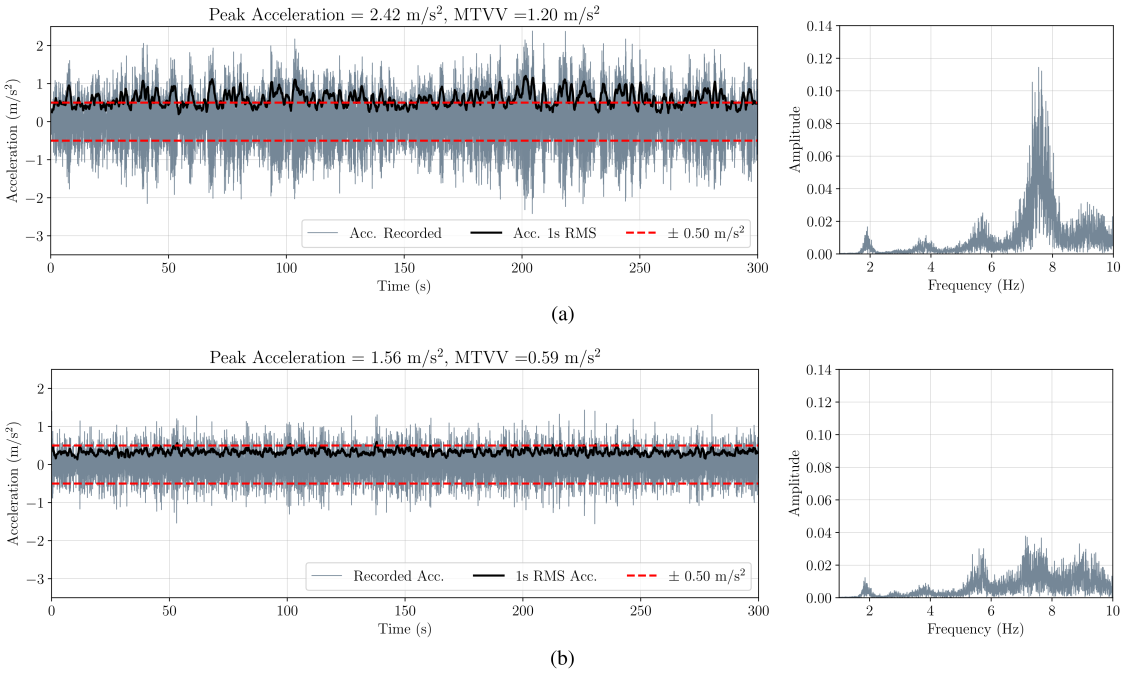

FIG. 12. Acceleration response of the FRP footbridge at midspan due to a dense TC: (a) Structure without control, and (b) Controlled structure with the TVA-25.

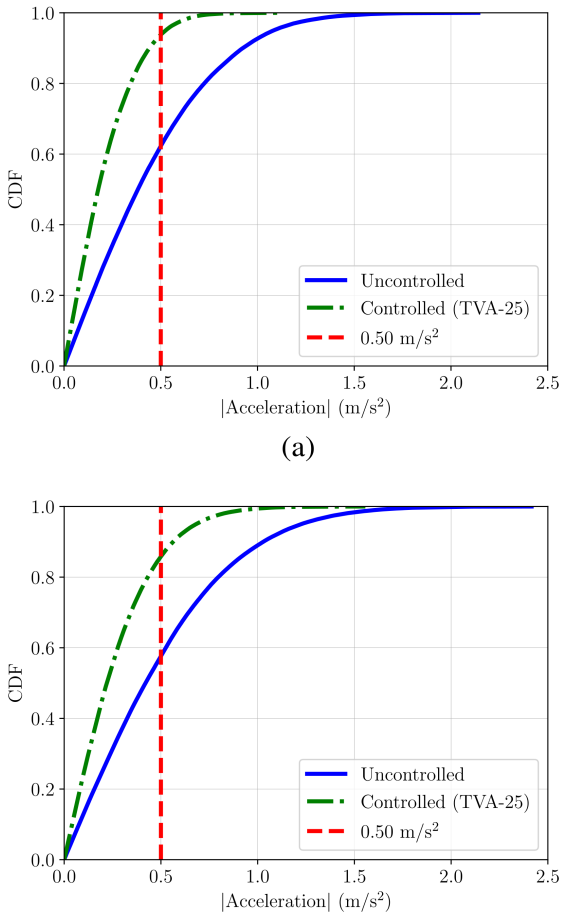

FIG. 13. CDF of the acceleration response of the FRP footbridge with the TVA-25: (a) Weak TC, and (b) Dense TC.